Neutralino annihilation into γ rays in the Milky Way and in external galaxies

N. Fornengo,[1,2,*] L. Pieri,[1,†] and S. Scopel[1,‡]

[1]*Dipartimento di Fisica Teorica, Università di Torino, via P. Giuria 1, I-10125 Torino, Italy*
[2]*Istituto Nazionale di Fisica Nucleare, Sezione di Torino, via P. Giuria 1, I-10125 Torino, Italy*

We discuss the gamma-ray signal from dark matter annihilation in our Galaxy and in external objects, namely, the Large Magellanic Cloud, the Andromeda Galaxy (M31), and M87. We derive predictions for the fluxes in a low energy realization of the minimal supersymmetric standard model and compare them with current data from EGRET, CANGAROO-II, and HEGRA and with the capabilities of new-generation satellite-borne experiments, like GLAST, and ground-based Čerenkov telescopes, like VERITAS. We find fluxes below the level required to explain the possible indications of a γ-ray excess shown by CANGAROO-II (toward the galactic center) and HEGRA (from M87). As far as future experiments are concerned, we show that only the signal from the galactic center could be accessible to both satellite-borne experiments and to atmospheric Čerenkov telescopes (ACTs), even though this requires very steep dark matter density profiles.

I. INTRODUCTION

The nature of the cold dark matter (CDM) which is believed to compose galactic halos is probably the most important open issue in present cosmology. A popular solution to this puzzle is given by the lightest supersymmetric particle (LSP) which, in most supersymmetry breaking scenarios, is the neutralino χ. In this case dark matter (DM) would be not so dark after all, since χ-χ annihilation is expected to lead, among other final states, to a γ signal which could in principle be detected above known backgrounds. In particular, since the neutralino annihilation rate is proportional to the square of its density, a signal enhancement is expected in high density regions like the center of our Galaxy or that of external ones, with the exciting possibility that such γ rays might be identified by forthcoming or just operating atmospheric Čerenkov telescopes (ACTs) such as VERITAS [1], HESS [2], and MAGIC [3] or by satellite-borne detectors like GLAST [4], let alone the even more intriguing chance that a hint of an exotic source of γ rays could actually be already present in the data of existing experiments, like EGRET [5] or CANGAROO-II [6]. However, assessing the size of such signals depends on many uncertain aspects of both astrophysics and particle physics. For instance, the central structure of the DM halos is far from being well determined, and this can lead to uncertainties in the calculation of expected γ rates spanning several orders of magnitude. Another sensitive issue is the presence of substructures in galactic halos, which can change predictions as compared to a smooth mass distribution.

The aim of the present paper is to investigate the possibility that neutralino annihilations in the halo of our galaxy [7–10], or that of external ones [11,12] (namely, the Large Magellanic Cloud, the Andromeda Galaxy, and M87) could produce detectable fluxes of γ rays. To this purpose we will discuss present astrophysical uncertainties and focus on deriving consistent predictions for these fluxes in a specific realization of supersymmetry, the effective minimal supersymmetric standard model (MSSM).

The plan of the paper is as follows: in Sec. II the main ingredients for the calculation of the γ-ray flux from neutralino annihilation are introduced; in Sec. III we discuss the contribution to the flux calculation coming from astrophysics, while in Sec. IV the contribution from particle physics is discussed, and the effective MSSM is outlined. In Sec. V we show our results and compare them to present data and the prospects of future experiments; finally, Sec. VI is devoted to our conclusions.

II. THE γ-RAY FLUX

The diffuse photon flux from neutralino annihilation in the galactic halo, coming from a given direction in the sky defined by the angle-of-view ψ from the galactic center, and observed by a detector with angular resolution θ can be written as:

$$\frac{d\Phi_\gamma}{dE_\gamma}(E_\gamma, \psi, \theta) = \frac{d\Phi^{\mathrm{SUSY}}}{dE_\gamma}(E_\gamma) \times \Phi^{\mathrm{cosmo}}(\psi, \theta). \quad (1)$$

The energy dependence in Eq. (1) is given by the annihilation spectrum:

$$\frac{d\Phi^{\mathrm{SUSY}}}{dE_\gamma}(E_\gamma) = \frac{1}{4\pi} \frac{\langle \sigma_{\mathrm{ann}} v \rangle}{2m_\chi^2} \sum_f \frac{dN_\gamma^f}{dE_\gamma} B_f \quad (2)$$

where $\langle \sigma_{\mathrm{ann}} v \rangle$ is the neutralino self-annihilation cross section times the relative velocity of the two annihilating particles, dN_γ^f/dE_γ is the differential photon spectrum for a given f-labeled annihilation final state with branch-

---
*Electronic address: fornengo@to.infn.it
†Electronic address: pieri@to.infn.it
‡Electronic address: scopel@to.infn.it

ing ratio B_f, and m_χ denotes the neutralino mass. The geometry dependence is given by the line-of-sight integral, defined as:

$$\Phi^{\text{cosmo}}(\psi, \theta) = \int_{\Delta\Omega(\psi,\theta)} d\Omega' \int_{\text{l.o.s}} \rho_\chi^2[r(\lambda, \psi')]d\lambda(r, \psi') \quad (3)$$

for the diffuse emission of our Galaxy, and

$$\Phi^{\text{cosmo}}(\psi, \theta) = \frac{1}{d^2} \int_0^{\min[R_G, r_{\max}(\Delta\Omega)]} 4\pi r^2 \rho_\chi^2(r)dr \quad (4)$$

for the emission from an extragalactic object located at the direction ψ. In Eq. (3), $\rho_\chi(r)$ is the dark matter density profile, r is the galactocentric distance, related to the distance λ from us by $r = \sqrt{\lambda^2 + R_\odot^2 - 2\lambda R_\odot \cos\psi}$ ($R_\odot$ is the distance of the Sun from the galactic center), and $\Delta\Omega(\psi, \theta)$ is the solid angle of observation pointing in the direction of observation ψ and for an angular resolution of the detector θ. Moreover, in Eq. (4) d is the distance of the external object from us, R_G is the radius of the external galaxy, and $r_{\max}(\Delta\Omega)$ is the maximal distance from the center of the external galaxy which is seen within the solid angle $\Delta\Omega(\psi, \theta)$. The quantity Φ^{cosmo}, expressed in units of $(\text{GeV}/\text{cm}^3)^2$ kpc sr, is related to the dimensionless parameter J of Ref. [13] by the simple relation $\Phi^{\text{cosmo}} = J \times 0.765 \times \Delta\Omega$.

We focus our attention on the fact that Eq. (1) is factorized into two distinct terms: a "cosmological factor" Φ^{cosmo} which takes into account the geometrical distribution of DM in the Universe, and a "supersymmetric factor" Φ^{SUSY} which contains the information about the nature of dark matter. In Secs. III and IV we will present results on the two factors separately.

III. THE COSMOLOGICAL FACTOR

In the following we present the determination of the cosmological factor Φ^{cosmo}, as defined in Eqs. (3) and (4). The dependence of Φ^{cosmo} on the astrophysical and cosmological details that we explore here is based on the determination of the shape of the dark matter halo. This takes into account the possible existence and prominence of central cusps, the study of the physical extent of the constant-density inner core, and the possible presence of a population of subhalos. We remind the reader that, for the moment, no definitive answer can be given to these questions by experimental constraints. In particular, the discussion about the possible existence of a halo with a cuspy behavior in its inner regions is still quite open. Moreover, theoretical predictions differ substantially among themselves, or take into account different input parameters.

These facts reflect themselves in a large uncertainty in the predictions of the gamma-ray fluxes arising from Φ^{cosmo}, as it is discussed and quantified in the following.

A. Modeling the Dark Matter Halo

The modeling of the DM density profile is an open question. It can be addressed through numerical N-body simulations whose scale resolution is about a few $\times 10^{-3} r_{100}$, where r_{100} is defined as the radius within which the halo average density is about $100\rho_c$ (ρ_c is the critical density). The very inner slope of the profile is then usually just extrapolated and does not take into account interactions with the baryons which fall in the DM potential well. A number of profiles have been proposed. Here we discuss some of the profiles which are compatible with observations and which we will use in our analysis.

In our calculation we mainly focus on the NFW profile (hereafter NFW97) [14]

$$\rho_\chi^{\text{NFW97}} = \frac{\rho_s^{\text{NFW97}}}{(r/r_s^{\text{NFW97}})(1 + r/r_s^{\text{NFW97}})^2} \quad (5)$$

and the Moore *et al.* profile (M99) [15]:

$$\rho_\chi^{\text{M99}} = \frac{\rho_s^{\text{M99}}}{(r/r_s^{\text{M99}})^{1.5}[1 + (r/r_s^{\text{M99}})^{1.5}]}. \quad (6)$$

The scale radii r_s^i and the scale densities ρ_s^i ($i = $ NFW97, M99) can be deduced by observations (the virial mass of the halo or the rotation curves) and by theoretical considerations that allow to determine the concentration parameter $c = r_{\text{vir}}/r_s$ (the virial radius r_{vir} is defined as the radius within which the halo average density is $200\rho_c$). The concentration parameters, c_{NFW97} and $c_{\text{M99}} = 0.64c_{\text{NFW97}}$, have been computed according to Ref. [16] with the assumption of a CDM power spectrum with a shape parameter $\Gamma = 0.2$ normalized to $\sigma_8 = 0.9$.

In addition to the two profiles mentioned before, we include in our predictions the conservative modified isothermal profile with a constant density core (isocore):

$$\rho_\chi^{\text{iso-core}} = \frac{\rho_s^{\text{iso-core}}}{[1 + (r/r_s^{\text{iso-core}})^2]} \quad (7)$$

and a profile which has been recently proposed by Moore and collaborators (M04) [17]:

$$\rho_\chi^{\text{M04}} = \frac{\rho_s^{\text{M04}}}{(r/r_s^{\text{M04}})^{1.16}(1 + r/r_s^{\text{M04}})^{1.84}}. \quad (8)$$

Figure 1 shows the comparison among the above mentioned profiles for the Milky Way, normalized to a local density of 0.3 GeV cm^{-3} and to $R_\odot = 8.5$ kpc. Two more profiles are shown for comparison on Fig. 1. One is the numerical profile obtained in Ref. [18] when the adiabatic growth of a central black hole is taken into consideration (adiab-NFW). This hypothesis of black-hole formation has been applied here to the NFW97 profile, and the density profile has been normalized as previously mentioned. The resulting profile has a behavior at the galactic center which is similar to the one of the M99 profile, therefore we will not discuss it in more detail. The last profile which is shown in the figure is a cored one recently
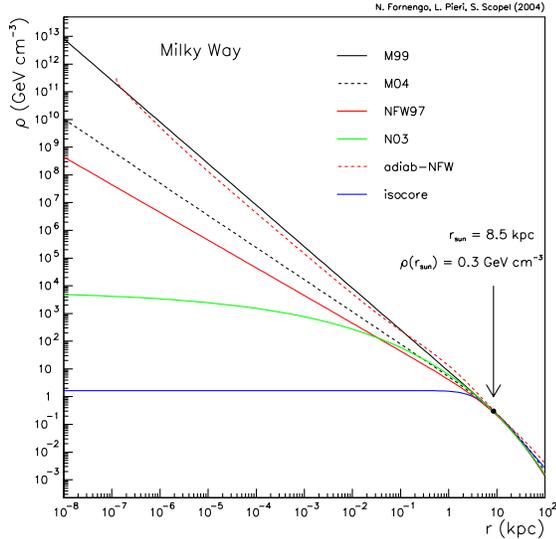
FIG. 1 (color online). Comparison between cuspy and cored dark matter density profiles for the Milky Way, as a function of the distance from the center of the Galaxy. All the curves are normalized to $\rho_0 \equiv \rho(R_\odot) = 0.3$ GeV cm^{-3}.

obtained in Ref. [19] (N03):

$$\rho_\chi^{\mathrm{N03}} = \rho_s^{\mathrm{N03}} \exp\left[-\frac{2}{\alpha}\left(\left(\frac{r}{r_s^{\mathrm{N03}}}\right)^\alpha - 1\right)\right] \qquad (9)$$

where $\alpha = 0.17$, $r_s^{\mathrm{N03}} = r_s^{\mathrm{NFW97}}$, and $\rho_s^{\mathrm{N03}} = \rho_s^{\mathrm{NFW97}}/4$. As noticed in Ref. [17], this profile is compatible with the M04 as far as the resolution of the N-body simulation holds. In the inner part of the Galaxy, it is an extrapolation which postulates the existence of a constant density core. Another recently proposed profile which does not exhibit singular behavior, and which has been shown to be able to reproduce to a good precision the rotational velocities of low surface brightness galaxies [20], is given in Ref. [21]. Predictions of gamma-ray fluxes for this profile are given in Ref. [9].

Since profiles shallower than the NFW97 hardly give observable fluxes of photons, we will not discuss it in detail. Studying the cored halos, we will limit ourselves to the isocore profile, which is pretty conservative.

Integrating the squared density along the line of sight introduces divergences when cuspy profiles are considered. Therefore we enforce a cutoff radius r_{cut} to the density profile, with a constant density core therein. The

TABLE I. Masses, distances and virial radii for the Milky Way, the LMC and M31.

Galaxy	mass ($M_\odot$)	distance (kpc)	r_{vir} (kpc)
MW	1.0×10^{12}	8.5	205
LMC	1.4×10^{10}	49	49
M31	2.0×10^{12}	770	258

TABLE II. Scale radii and scale densities for the NFW97, M99, M04, and isocore density profiles calculated for the Milky Way.

Profile	scale radius r_s (kpc)	scale density ρ_s ($M_\odot$kpc^{-3})
NFW97	21.746	5.376×10^6
M99	34.52	1.060×10^6
M04	32.625	2.541×10^6
isocore	4	7.898×10^6

smallest value for the cutoff radius which we will use is $r_{\mathrm{cut}} = 10^{-8}$ kpc, a value we will discuss in the next section, where the effect of varying r_{cut}, both for our Galaxy and for the external ones, will be discussed.

The analysis of Ref. [11] shows that a number of external galaxies shine above the galactic foreground. In the following we will focus on the two most prominent galaxies at large angles with respect to the galactic center, namely, the Large Magellanic Cloud (LMC) and the Andromeda Galaxy (M31) [11]. Table I shows the astrophysical parameters for the Milky Way, the LMC, and M31, while Tables II, III, and IV show the scale radius and the scale density parameters used in our calculations.

1. Comment on the experimental constraints on the inner part of galaxies

As we have seen, theoretical estimates of the inner slope α of the DM density profile $\rho(r) \propto r^{-\alpha}$ are still uncertain. Moreover, observations which should constrain the α parameter do not give clear and definitive answers on its value. A number of works give in fact non-unique values for the slope.

In Ref. [22] spatially resolved spectra of the diffuse hot (x rays) gas of galaxies and clusters measured with the Chandra satellite were used to infer the radial mass distribution of the considered systems. An analysis was done on two clusters which are relaxed in their cores on $O(10^2$ kpc$)$ to O(Mpc) scales and do not have strong radio sources in their center. Resulting values for α are 1.25 and 1.35. A value of α less than 1 is found when disturbed x-ray surface brightness clusters are used. Yet the x-ray method uses the double assumption of a single phase gas in hydrostatic equilibrium, which for instance is questionable in the central regions where rapid cooling occurs.

TABLE III. Scale radii and scale densities for the NFW97, M99, M04, and isocore density profiles calculated for the LMC.

Profile	scale radius r_s (kpc)	scale density ρ_s ($M_\odot$kpc^{-3})
NFW97	4.353	8.50×10^6
M99	6.8	1.80×10^6
M04	6.426	3.22×10^6
isocore	1.5	2.17×10^7

TABLE IV. Scale radii and scale densities for the NFW97, M99, M04, and isocore density profiles calculated for M31.

Profile	scale radius r_s (kpc)	scale density ρ_s ($M_\odot$kpc^{-3})
NFW97	30.271	4.20×10^6
M99	47.298	0.86×10^6
M04	44.697	1.55×10^6
isocore	4	7.898×10^6

Other studies of radial mass profiles inferred by the radial profile of the intracluster medium density and temperature measured with Chandra can be found in Ref. [23] where the analysis of five clusters gives $1 < \alpha < 2$.

Different results are found by Ref. [24] using low surface brightness (LSB) galaxies' rotation curves. Fits to their measured curves give a mean value $\langle\alpha\rangle = 0.2$, although tails in the distribution extend further, up to $\alpha = 2$. In Ref. [25] a combination of strong-lensing data and spectroscopic measurements of stellar dynamics of the brightest cluster galaxies was used to derive values of α. Three clusters, containing both radial and tangential arcs, have been found. The obtained distribution gives $\langle\alpha\rangle = 0.52$ with $\Delta\alpha = 0.3$.

In Ref. [26] the full radial extent of LSB galaxies' rotation curves, instead of their inner portions, was used to determine the inner slope of the DM density profile. Convergence criteria for the N-body simulations taken from Ref. [27] give a minimum radius for which simulations are reliable, $r_{conv} = 1h^{-1}$ kpc. It is shown that, at that radius, 2/3 of the sample in Ref. [24] is consistent with a profile which lies between the simulated NFW97 and M99 ones. There are inconsistencies with CDM predictions in those galaxies which show a sharp transition between the rising and flat part of the rotation curve. This is due to the fact that rotation curves of gas disks are compared with the spherically-averaged circular velocity profiles of DM halos. This assumption may not be correct in non-regular galaxies.

Another study of high resolution H_α rotation curves for dwarf and LSB galaxies has been recently carried out in Ref. [28]. In that work it is shown that rotation curve data are insufficient to rule out halos with $\alpha = 1$, although none of the galaxies require an inner cuspy profile instead of a core density feature. Results on α range from 0 to 1.2, although the quality of the fit is good only up to $\alpha = 1$. Other analyses on large sets of data of high-resolution rotation curves also show consistency with cored mass distributions [29].

An indirect estimate of α can be inferred through the weak gravitational lensing measurements of x-ray luminous clusters [30]: one finds $0.9 < \alpha < 1.6$.

The analysis of the microlensing optical depth toward the galactic center was performed in Ref. [31]. Assuming a naïve spherically symmetric profile normalized to our position in the Milky Way, the authors find $\alpha = 0.4$. They argue that the value $\alpha = 1$ can be reached by considering a flattened halo with a ratio of polar to equatorial axis of 0.7.

2. Comment on the unknown effect of baryons on the inner part of galaxies

Dark matter density profiles obtained in N-body simulations do not always take into account the effect that baryons can have in the formation or disruption of the central cusp.

The numerical adiab-NFW profile shown in Fig. 1, for instance, takes into account the effect of the adiabatic growth of a central black hole, which pulls in DM and enhances the spike of an initial NFW97 profile. Spikes in the center of the DM halo could in principle be created either by the growth of a black hole [32] or by the dissipation of the baryons which steepens the radial profile in the inner regions of the DM halo [33,34]. In Ref. [33] a high-resolution cosmological simulation which includes the effects of baryons cooling, gas dynamics, and star formation has been performed. The results show that, by starting from an NFW97 profile, the inner slope could sizably increase and reach the value of $\alpha \sim 1.6$ at $r \lesssim 0.1 r_{vir}$. Following the same line, the authors of Ref. [34] find that the effect of baryon cooling on an NFW97 initial profile could lead to an enhancement of the expected γ-ray flux from the galactic center of more than 3 orders of magnitude.

It is worth noticing, however, that if the central supermassive black hole (SBH) is formed by the merging of halos hosting SBHs, the subsequent formation of an SBH binary would lead to a depletion of the central spike, because DM particles would be given enough energy to be thrown out of the system. The final slope would then result in a shallower profile with $\alpha \sim 0.5$ [35]. Also, as shown in Refs. [36,37], the central spike due to the presence of a black hole could be dissolved by the interaction of DM with the population of stars, due both to the kinetic heating of the DM by stars, and to the DM capture by the SBH, as an effect of scattering into an eccentric orbit around the SBH. The authors of Refs. [36] find that this effect results in a depletion of the expected γ-ray flux of even up to 6 orders of magnitude, depending on the initial slope of the spiky profile.

All these effects stress the uncertainty in the astrophysical/cosmological modeling of the problem, and show how much attention must be paid when comparing predictions to data.

B. Including the effect of the inner core

There exists a physical minimal radius, r_{cut}, within which the self-annihilation rate $t_l \sim [\langle\sigma_{ann}v\rangle n_\chi(r_{cut})]^{-1}$ equals the dynamical time $t_{dyn} \sim (G\bar\rho)^{-1/2}$ [38], where $\bar\rho$ is the mean halo density and n_χ is the neutralino number

density. When this procedure is applied to the density profiles we are using, the evaluated r_{cut} are of the order of 10^{-8} to 10^{-9} kpc for the M99 profile and of 10^{-13} to 10^{-14} kpc for an NFW97. Another estimation of the minimum physical radius can be inferred by taking into account the effect of baryons. The presence of a central black hole would reduce the central density of DM particles, which are lost inside a radius of the order of about 3×10^{-10} kpc for the Milky Way and 3×10^{-7} kpc for M87. Moreover, it has been shown [36] that scattering of DM particles into the black hole by stars could imply a vanishing DM density below a radius of the order of a few $\times 10^{-9}$ kpc.

Evaluating the constant core is indeed a much more complicated issue. Taking into account additional effects, especially tidal interactions, the central core of galaxies can significantly exceed the values quoted above, reaching values as large as $\mathcal{O}(0.1 - 1)$ kpc [39]. We want to remind that also numerical simulations, from which the cuspy behavior is deduced for the inner parts by means of extrapolation, are actually testing the halo shape down to $\mathcal{O}(0.1)$ kpc [17,19].

In our analysis we will take into account this large uncertainty in the inner core radius by varying r_{cut} in the range $[10^{-8}, 10^{-1}]$ kpc.

C. Results for Φ^{cosmo}

The results of the calculations of the cosmological factor Φ^{cosmo} for the Milky Way are shown in Fig. 2, for the four main profiles previously discussed and for a detector with angular resolution equal to 1° and 0.1°. A constant-density central region of radius $r_{cut} = 10^{-8}$ kpc has been used for the cuspy profiles. Since the value of r_{cut} used in Fig. 2 somehow represents a lower bound on the acceptable values of this parameter, the values of Φ^{cosmo} shown in Fig. 2 can be taken as an upper bound on the cosmological factor, for any given halo profile and for the two representative acceptance angles. Clearly the non-cuspy profiles are not affected by the choice of r_{cut}.

In the same figure, the values of Φ^{cosmo} for LMC and M31 are also shown. We see that these external galaxies can be resolved against the galactic signal in all cases, except for the case of LMC with an isocore density profile. These two external galaxies can therefore be looked at as gamma-ray sources from DM annihilation (provided that the ensuing gamma-ray flux can be detected against the gamma-ray background). If a gamma-ray signal were detected, for instance from the galactic center, it should be correlated to a corresponding signal both from LMC and from M31. Since the supersymmetric factor is the same for all the sources, the relative strength of the gamma-ray fluxes from the galactic center, LMC, and M31, could then be used to deduce information on the halo shape, since it depends only on the DM density profile. However, this possibility is strongly limited by

the fact that Φ^{cosmo} for LMC and M31 is much smaller than the one from the galactic center, as is clear from Fig. 2. The ensuing fluxes from external galaxies will therefore be much smaller than the ones from the galactic center.

The dependence of the cosmological factor on the cut-off radius of the inner core is shown in Fig. 3 for the Milky Way and in Fig. 4 for LMC and M31. In these figures we plot the ratio $\Phi^{cosmo}(\text{profile}, r_{cut}, \psi)/$
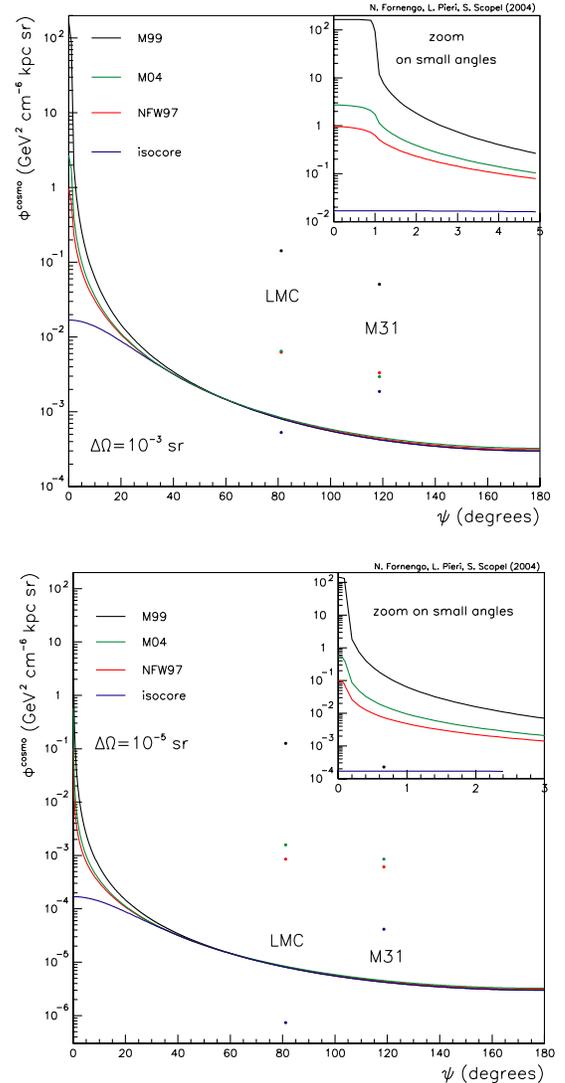

FIG. 2 (color online). The lines denote the cosmological factor Φ^{cosmo} for the Milky Way, calculated for different dark matter profiles, for a solid angle $\Delta\Omega = 10^{-3}$ sr (upper panel) and $\Delta\Omega = 10^{-5}$ sr (lower panel). The insets show a zoom at small angles toward the galactic center. A constant-density central region of radius $r_{cut} = 10^{-8}$ kpc has been used for the cuspy profiles. The points at $\psi \simeq 81°$ and $\psi \simeq 119°$ denote the values of Φ^{cosmo} for LMC and M31, respectively. From top to bottom the points refer to different halo profiles: Moore, NFW97, M04, and isocore in the upper panel; Moore, M04, NFW97, and isocore in the lower panel.
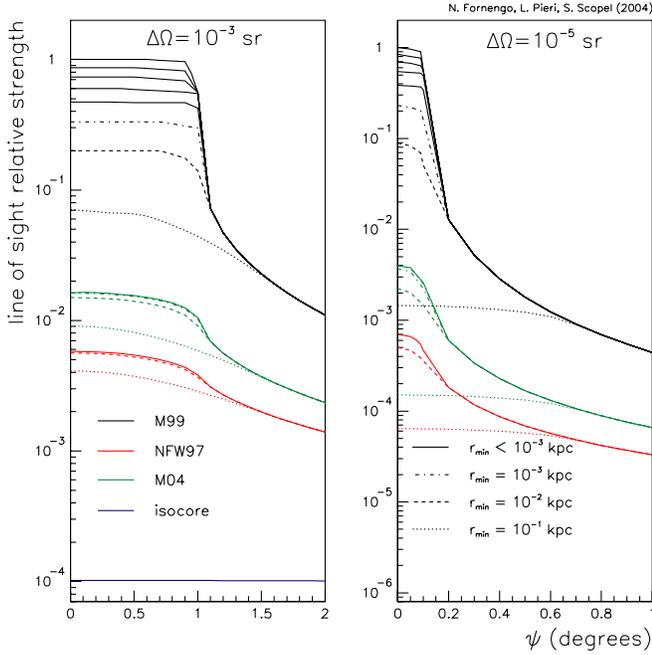
FIG. 3 (color online). Relative strength of the line-of-sight integral with respect to different halo profiles and different inner core radii for the Milky Way. Numbers are normalized to the highest value of the Φ^{cosmo} given by an M99 profile with a physical cutoff radius of 10^{-8} kpc and at $\psi = 0$. Left panel: solid angle $\Delta\Omega = 10^{-3}$ sr. Right panel: solid angle $\Delta\Omega = 10^{-5}$ sr.
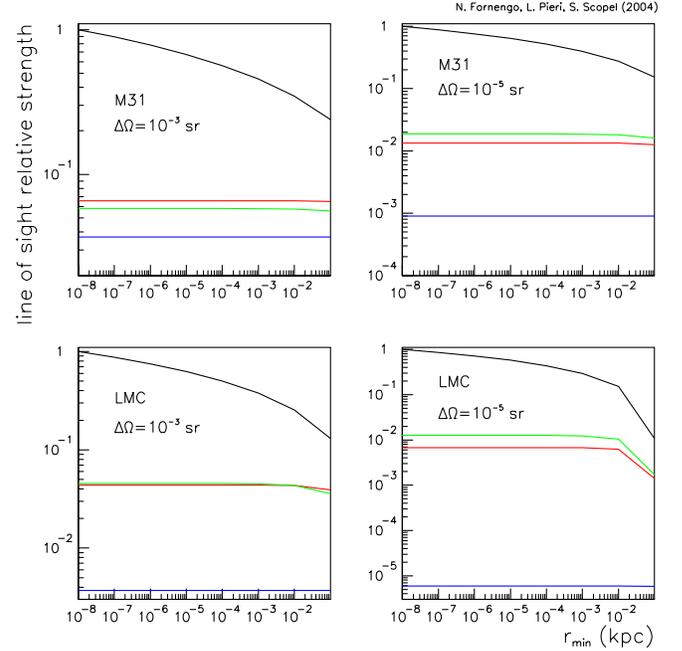

FIG. 4 (color online). Relative strength of the line-of-sight integral with respect to different halo profiles and different inner core radii for M31 (upper panels) and the LMC (lower panels). Numbers are normalized to the highest value of the Φ^{cosmo} given by an M99 profile with a physical cutoff radius of 10^{-8} kpc and at $\psi = 0$. Left panels: solid angle $\Delta\Omega = 10^{-3}$ sr. Right panels: solid angle $\Delta\Omega = 10^{-5}$ sr.

Φ^{cosmo}(M99, $r_{cut} = 10^{-8}$ kpc, $\psi = 0$) for the M99, NFW97, M04, and isocore profiles and for r_{cut} in the range discussed above . As expected, a cored distribution or a less cuspy profile than the M99 decreases the cosmological factor by a significant amount with respect to the most optimistic hypotheses of an M99 profile with an inner core radius $r_{cut} = 10^{-8}$ kpc. Figures 3 and 4 quantify this effect.

In the case of the Milky Way, the reduction factor at the galactic center can be sizable: for instance, when an NFW97 profile with $r_{cut} = 0.1$ kpc is used, the reduction is of the order of 4×10^{-3} for a solid angle of observation $\Delta\Omega = 10^{-3}$ sr and 6×10^{-5} for $\Delta\Omega = 10^{-5}$ sr. In the case of the isocored distribution the reduction factor is as large as 10^{-4} for $\Delta\Omega = 10^{-3}$ and 10^{-6} for $\Delta\Omega = 10^{-5}$.

The same trend is observed for the external galaxies which we have considered, although the net effect is less prominent. In the case of M31, the reduction is at most a few $\times 10^{-2}$ for $\Delta\Omega = 10^{-3}$ and it can reach 10^{-3} for $\Delta\Omega = 10^{-5}$ and the isocore profile. For LMC, the reduction is again of the order of 10^{-2} to 10^{-3}, except for the isocore profile and $\Delta\Omega = 10^{-5}$, for which it reaches values of the order of 10^{-5}.

In the following, for definiteness we will refer to the most optimistic values of Φ^{cosmo} shown in Fig. 2, obtained for an M99 profile with a cutoff radius of 10^{-8} kpc and to an NFW97 shape, with the same cutoff radius.

Results for different halo profiles or core parameters can be easily obtained by scaling the results according to Figs. 3 and 4.

D. Including substructures

In the CDM scenario, subhalos that accrete into larger systems are tidally stripped of a fraction of their mass, originating debris streams [40]. Their dense central cores, however, survive the merging event and continue to orbit within the parent halo. High resolution N-body simulations [15,41] have indeed shown that DM halos host a population of subhalos with a distribution function depending on the subhalo mass and on the distance of the subhalo from the halo center [42].

The effect of including subhalos in the Milky Way and in the galaxies of the local group has been discussed in Refs. [11,43–45], where different parameters for the subhalo distribution, along with the existence of mass stripping and tidal heating, have been considered, and a minimum mass of $10^6 M_\odot$ was assumed for the subhalos. The existence of such a subhalo population leads to average boost factors for expected rates which depend on the modeling of the subhalo distribution and on the density profile, and can range from few unities to more than 10^4. In no case, however, is the field of view toward the galactic center affected, since in that region the gravita-

tional strengthening reduces the probability of finding subhalos. The total effect of the presence of subhalos in external galaxies is limited to a factor 2–5.

A discussion on the minimum mass of subhalos in our Galaxy can be found in Ref. [39], where small scale clumps are considered, with masses down to $10^{-8}M_\odot$ for a DM constituted by neutralinos. An average enhancement factor of 2–5 is found, depending on the profile, while the enhancement toward the galactic center is found to be of a factor ~ 0.3 (NFW97) to ~ 0.5 (M99).

Hereafter we consider values for the cosmological factor related to an unclumpy scenario. For a clumpy halo our results can be scaled according to the previous considerations.

IV. THE SUPERSYMMETRIC FACTOR

In our study we employ a minimal supersymmetric extension of the standard model (MSSM), which is defined as an effective theory at the electroweak scale. The scheme is defined in terms of a minimal number of parameters, only the ones which are necessary to shape the essential properties of the theoretical structure of the MSSM and of its particle content. A number of assumptions are therefore imposed at the electroweak scale: (a) all squark soft-mass parameters are degenerate: $m_{\tilde{q}_i} \equiv m_{\tilde{q}}$; (b) all slepton soft-mass parameters are degenerate: $m_{\tilde{l}_i} \equiv m_{\tilde{l}}$; (c) all trilinear parameters vanish except those of the third family, which are defined in terms of a common dimensionless parameter A: $A_{\tilde{b}} = A_{\tilde{t}} \equiv A m_{\tilde{q}}$ and $A_{\tilde{\tau}} \equiv A m_{\tilde{l}}$. In addition, we employ also the standard relation at the electroweak scale between the U(1) and SU(2) gaugino mass parameters: $M_1 = (5/3)\tan^2\theta_W \simeq 0.5\, M_2$, which is the low energy consequence of an underlying unification condition for the gaugino masses at the grand unified theory (GUT) scale. In this class of gaugino-universal models, the neutralino mass has a lower bound of about 50 GeV. This limit is induced by the lower bound on the chargino mass determined at LEP2 [46]: $m_{\chi^\pm} \gtrsim 100$ GeV. This is at variance with respect to effective MSSM schemes which do not possess gaugino-universality, where the neutralino mass can be as low as a few GeV's (see, for instance, Refs. [7,47] and references quoted therein). Gamma-ray detection from the annihilation of these light neutralinos has also been analyzed in Ref. [10], in the context of supergravity (SUGRA) models where gaugino nonuniversality is defined at the GUT scale.

Because of the above mentioned assumptions, the supersymmetric parameter space of our scheme consists of the following independent parameters: M_2, μ, $\tan\beta$, m_A, $m_{\tilde{q}}$, $m_{\tilde{l}}$ and A. In the previous list of parameters μ denotes the Higgs mixing mass parameter, m_A is the mass of the CP-odd neutral Higgs boson and $\tan\beta \equiv v_t/v_b$ is the ratio of the two Higgs vacuum expectation values (VEVs) that give mass to the top and bottom quarks.

When we perform a numerical random scanning of the supersymmetric parameter space, we employ the following ranges for the parameters: $1 \leq \tan\beta \leq 50$, 100 GeV $\leq |\mu|$, $M_2 \leq 6000$ GeV, 100 GeV $\leq m_{\tilde{q}}, m_{\tilde{l}} \leq$ 3000 GeV, sgn$(\mu) = -1, 1$, 90 GeV $\leq m_A \leq 1000$ GeV, $-3 \leq A \leq 3$. The range on both M_2 and μ extends up to 6 TeV in order to allow us to study also very heavy neutralinos, with a mass up to about 3 TeV.

The parameter space of our effective MSSM is constrained by many experimental bounds: accelerator data on supersymmetric and Higgs boson searches [48] and on the invisible width of the Z boson, measurements of the branching ratio of the $b \rightarrow s + \gamma$ decay and of the upper bound on the branching ratio of $B_s \rightarrow \mu^+ + \mu^-$, and measurements of the muon anomalous magnetic moment $a_\mu \equiv (g_\mu - 2)/2$. The limits we use are: $2.18 \times 10^{-4} \leq BR(b \rightarrow s + \gamma) \leq 4.28 \times 10^{-4}$ [49]; $BR(B_s \rightarrow \mu^+ + \mu^-) < 7.5 \times 10^{-7}$ (95% C.L.) [50]; $-142 \leq \Delta a_\mu \times 10^{11} \leq 474$ (this 2σ C.L. interval takes into account the recent evaluations of Refs. [51,52]).

For the theoretical evaluation of $BR(b \rightarrow s + \gamma)$ and $BR(B_s \rightarrow \mu^+ + \mu^-)$ we have used the results of Ref. [53,54], respectively, with inclusion of the QCD radiative corrections to the bottom-quark Yukawa coupling discussed in Ref. [55]. We notice that gluinos do not enter directly into our loop contributions to $BR(b \rightarrow s + \gamma)$ and $BR(B_s \rightarrow \mu^+ + \mu^-)$, since we assume flavor-diagonal sfermion mass matrices. Gluinos appear only in the QCD radiative corrections to the b Yukawa coupling: in this case M_3 is taken at the standard unification value $M_3 = M_2 \alpha_3(M_Z)/\alpha_2(M_Z)$, where $\alpha_3(M_Z)$ and $\alpha_2(M_Z)$ are the SU(3) and SU(2) coupling constants evaluated at the scale M_Z.

Another relevant observational constraint comes from cosmology. The recent observations on the cosmic microwave background from WMAP [56], used in combination with galaxy surveys, Lyman-α forest data, and the Sloan Digital Sky Survey Collaboration results [57], are leading to a precise knowledge of the cosmological parameters, and, in particular, of the amount of dark matter in the Universe. From the analysis of Ref. [56], we can derive a restricted range for the relic density of a cold species like the neutralinos. The density parameter of cold dark matter is bounded at 2σ level by the values: $(\Omega_{CDM}h^2)_{min} = 0.095$ and $(\Omega_{CDM}h^2)_{max} = 0.131$. This is the range for CDM that we consider in the present paper. For supersymmetric models which provide values of the neutralino relic abundance $\Omega_\chi h^2$ smaller than the minimal value $(\Omega_{CDM}h^2)_{min}$, i.e., for models where the neutralino represents a subdominant DM component, we accordingly rescale the value of the DM density: $\rho_\chi(r) = \xi \rho(r)$ with $\xi = \Omega_\chi h^2/(\Omega_{CDM}h^2)_{min}$.

We recall that the relic abundance $\Omega_\chi h^2$ is essentially given by $\Omega_\chi h^2 \propto \langle \sigma_{ann} v \rangle_{int}^{-1}$, where $\langle \sigma_{ann} v \rangle_{int}$ is the thermal-average of the product of the neutralino annihi-

lation cross section and velocity, integrated from the freeze-out temperature in the early Universe down to the present one. The analytical calculation of σ_{ann} relies on the full set of available final states: fermion-antifermion pairs, gluon pairs, Higgs boson pairs, one Higgs boson and one gauge boson, and pairs of gauge bosons [58]. We have not included coannihilation [59] in our evaluation of the neutralino relic abundance, since in our effective supersymmetric model a matching of the neutralino mass with other particle masses is usually accidental, and not induced by some intrinsic relationship among the different parameters of the supersymmetric model like, instead, in a constrained SUGRA scheme. The inclusion of coannihilation would not change the main results of our analysis, since it would only reflect in a limited reshuffle of a small fraction of the points of the scatter plots displayed in the next sections.

A. The annihilation cross section

As already stated in Sec. II, the gamma-ray flux produced by neutralino annihilation depends on the thermal average of the neutralino self-annihilation cross section $\langle \sigma_{ann} v \rangle$ in the galactic halo at present time. The behavior of $\langle \sigma_{ann} v \rangle / m_\chi^2$, which is a relevant quantity in the calculation of the gamma-ray flux, is shown in Fig. 5 as a function of the neutralino mass and for the effective MSSM we are using. We remind that $\langle \sigma_{ann} v \rangle$ in general
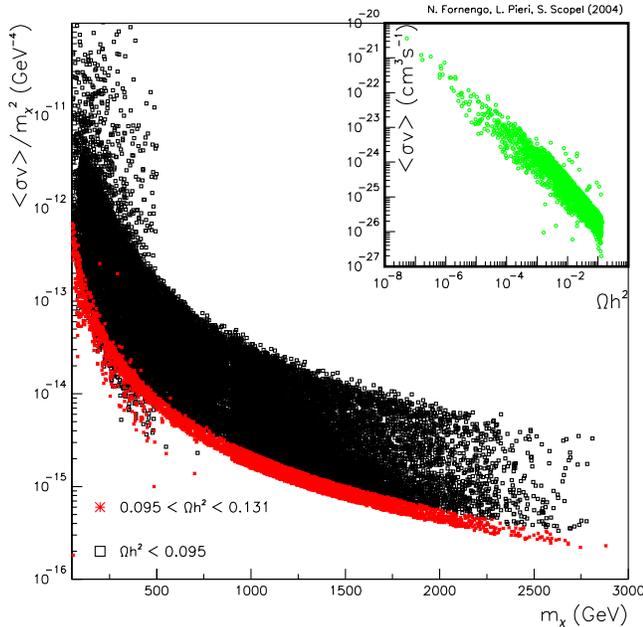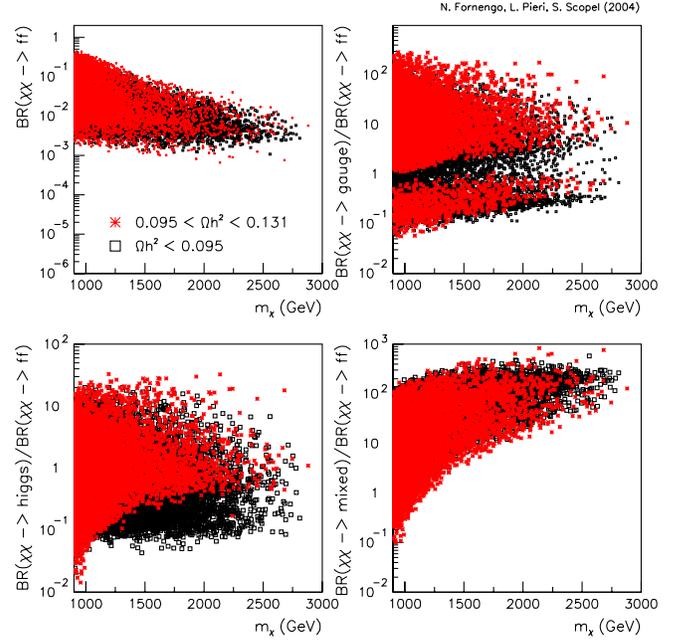

FIG. 6 (color online).   The upper left panel shows the branching ratios for high mass neutralino annihilation into fermions. The other three panels show the strength of annihilation into gauge bosons (upper right), Higgs bosons (lower left), and gauge + Higgs bosons (lower right) relative to annihilation into fermions.

is different from $\langle \sigma_{ann} v \rangle_{int}$ which is responsible for the determination of the relic abundance. The two cross sections closely follow each other only for s-wave annihilation. An inverse proportionality between the gamma-ray signal and the relic abundance is therefore usually a good approximation, although deviations are present. This effect is shown in the inset of Fig. 5.

Other key ingredients for the determination of the gamma-ray signal are the branching ratios of the annihilation cross section into the different final states. For neutralinos lighter than 1 TeV the branching ratios were shown in Ref. [60]. Figure 6 extends the behavior of the branching ratios for neutralino masses higher that 1 TeV. We see that in this case the dominant channels are the two gauge bosons and the gauge boson + Higgs boson final states.

B. The photon spectrum

The diffuse photon spectrum from neutralino annihilation originates from the production of fermions, gauge bosons, Higgs bosons, and gluons. Both gauge bosons and Higgs bosons eventually decay into fermions. The hadronization of quarks and gluons, in addition to radiative processes, can produce γ rays. The main channel of production of γ rays goes through the production and subsequent decay of neutral pions. The contribution to the γ-ray spectrum from production and decay of mesons other than pions (mostly η, η', charmed, and bottom

FIG. 5 (color online).   The thermally-averaged annihilation cross section divided by the square of the neutralino mass m_χ as a function of m_χ in the frame of the eMSSM. Crosses show the WMAP-preferred zone for a DM dominant neutralino. In the inset the annihilation cross section at the present epoch is shown as a function of the neutralino relic abundance.

mesons) and of baryons is usually subdominant as compared to π^0 decay and it has been neglected. Neutralino annihilation into lepton pairs can also produce γ rays from electromagnetic showering of the final state leptons. This process can be dominant for $E_\gamma \lesssim 100$ MeV, when the neutralino annihilation process has a sizable branching ratio into lepton pairs. In the case of production of τ leptons, their semihadronic decays also produce neutral pions, which then further contribute to the gamma-ray flux.

As discussed in Ref. [7], we have evaluated the gamma-ray fluxes originating from hadronization and radiative processes by means of a Monte Carlo simulation with the PYTHIA package [61]. In the present paper we extend that analysis by giving explicit fits to our numerical distributions which are valid for the energies of interest in the current analysis, i.e., for photon energies $E > 10$ GeV. When a flux is presented for energies below 10 GeV, the numerical analysis has been used.

The differential spectra of photons from DM annihilation have been parametrized as follows:

$$\frac{dN_\gamma^i}{dx} = \eta x^a e^{b + cx + dx^2 + ex^3} \qquad (10)$$

where $x = E_\gamma/m_\chi$ and i identify quarks, W, Z and gluons. The value of η is two for W, Z and top quark final states, and one otherwise. In the case of τ leptons, the functional

TABLE V. Fitted parameters of Eq. (10) for the annihilation of neutralinos into quarks and gauge bosons, calculated for $m_\chi = 500$ GeV and $m_\chi = 1$ TeV. Fits obtained with these parameters are valid down to $E = 10$ GeV.

	$m_\chi = 500$ GeV			$m_\chi = 1$ TeV		
	u	s	t	u	s	t
a	-1.5	-1.5	-1.5	-1.5	-1.5	-1.5
b	0.047	0.093	-0.44	0.0063	0.040	-0.45
c	-8.70	-9.13	-19.50	-8.62	-8.84	-19.05
d	9.14	4.49	22.96	8.53	2.77	21.96
e	-10.30	-9.83	-16.20	-9.73	-7.71	-15.18
	d	c	b	d	c	b
a	-1.5	-1.5	-1.5	-1.5	-1.5	-1.5
b	0.047	0.25	0.48	0.0063	0.17	0.37
c	-8.70	-10.76	-16.87	-8.62	-10.23	-16.05
d	9.14	4.25	21.09	8.53	2.13	18.01
e	-10.30	-8.70	-22.49	-9.73	-7.00	-19.50
	W	Z	g	W	Z	g
a	-1.5	-1.5	-1.5	-1.5	-1.5	-1.5
b	-0.85	-0.76	0.55	-0.95	-0.83	0.48
c	-11.07	-11.96	-20.78	-9.86	-11.175	-20.51
d	9.47	8.65	26.79	6.25	6.5902	24.42
e	-6.80	-5.21	-22.80	-4.37	-3.6468	-19.56

TABLE VI. Parameters of Eq. (11) for the annihilation of neutralinos into τ leptons, calculated for $m_\chi = 500$ GeV and $m_\chi = 1$ TeV. Fits obtained with these parameters are valid down to $E = 10$ GeV.

	$m_\chi = 500$ GeV	$m_\chi = 1$ TeV
a_τ	-1.34	-1.31
b_τ	6.27	6.94
c_τ	0.89	-4.93
d_τ	-4.90	-0.51
e_τ	-5.10	-4.53

form for the differential number of photons is:

$$\frac{dN_\gamma^\tau}{dx} = x^{a_\tau}(b_\tau x + c_\tau x^2 + d_\tau x^3)e^{e_\tau x}. \qquad (11)$$

The values of the parameters of the fits are given in Tables V and VI for the two representative values of $m_\chi = 500$ GeV and $m_\chi = 1$ TeV.

In Fig. 7 we show an example of photon spectra originated by neutralino annihilation into different pure final states of a neutralino with $m_\chi = 1$ TeV. We see that at lower energies the dominant contribution is given by the γ rays coming from the hadronization of quarks and gluons. The spectra coming from gauge bosons are somewhat harder, while the hardest ones are given by the τ lepton. In the case of Higgs bosons, the spectra are mainly
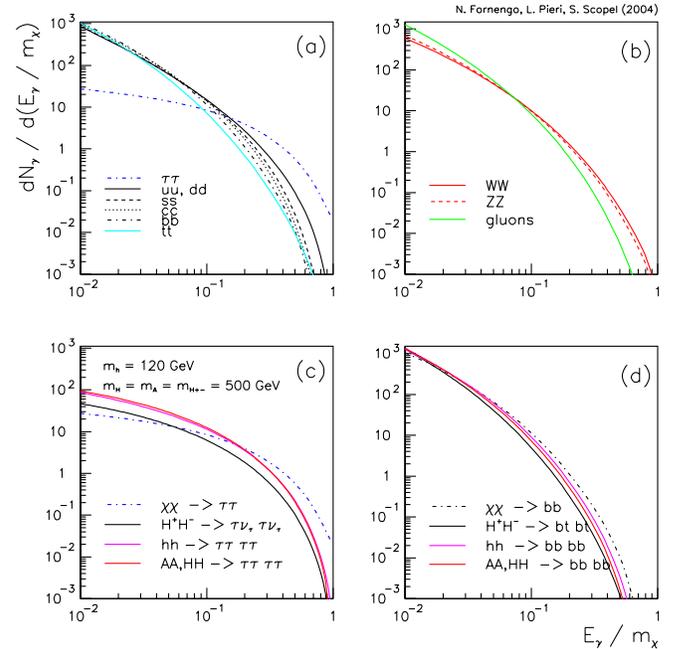

FIG. 7 (color online). The photon spectrum from an $m_\chi = 1$ TeV neutralino annihilation into: (a) leptons, (b) gauge bosons, (c) Higgs bosons decaying into τ's, and (d) Higgs bosons decaying into b's. For each curve a branching ratio of 100% in that channel has been considered.

driven by the type of particle in which the Higgs bosons decays, and are somewhat softer.

C. Results on Φ^{SUSY}

The composition of the information on the neutralino annihilation cross section and branching ratios with the informations coming from the differential spectra of photons from the annihilation of neutralinos in pure final states provides the prediction of what we have called the supersymmetric factor Φ^{SUSY} in the γ-ray flux computation. Figure 8 shows Φ^{SUSY} defined as the integral of the gamma-ray flux of Eq. (2) above a set of sample threshold energies: 1, 10, 50, and 100 GeV. When the threshold energy is small, Φ^{SUSY} is roughly inversely proportional to the neutralino mass. Since the neutralinos annihilate almost at rest, when the threshold energy increases Φ^{SUSY} significantly drops because the highest available photon energy is $E \sim m_\chi$ for any given neutralino mass. The highest value for Φ^{SUSY} is of the order of 10^{-8} cm^4 kpc^{-1} s^{-1} GeV^{-2} sr^{-1} when the threshold energy is 1 GeV. At masses larger than about 500 GeV for any given threshold energy the values of Φ^{SUSY} all lie inside a band which spans no more than 1 order of magnitude. This makes the predictions on the gamma-ray fluxes for large neutralino masses quite predictive: the possible variation due to the different supersymmetric models is confined to a relatively restricted range, much smaller than for the case of lighter neutralinos.

The information on the factor Φ^{SUSY} is detailed in Tables VII, VIII, and IX where we give the number of
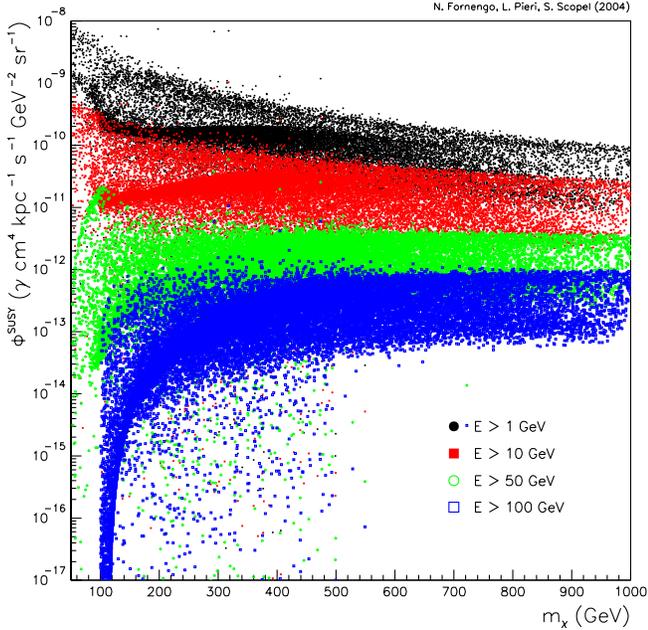

FIG. 8 (color online). The supersymmetric factor Φ^{SUSY} as a function of the neutralino mass. Different colors show different threshold energies above which the energy spectra have been integrated.

TABLE VII. Integrated number of photons above a given energy E from the annihilation of neutralinos with masses 500 GeV, 800 GeV, and 1 TeV, for different channels of annihilation.

	$m_\chi = 500$ GeV	$m_\chi = 800$ GeV	$m_\chi = 1$ TeV
$\chi\chi \longrightarrow u\bar{u}$ $(d\bar{d})$			
$N_\gamma(>10$ GeV$)$	6.65	9.79	11.63
$N_\gamma(>50$ GeV$)$	0.91	1.78	2.37
$N_\gamma(>100$ GeV$)$	0.23	0.59	0.87
$N_\gamma(>500$ GeV$)$	0.00	1.9×10^{-3}	8.4×10^{-3}
$\chi\chi \longrightarrow s\bar{s}$			
$N_\gamma(>10$ GeV$)$	6.61	9.83	11.71
$N_\gamma(>50$ GeV$)$	0.76	1.62	2.21
$N_\gamma(>100$ GeV$)$	0.15	0.46	0.73
$N_\gamma(>500$ GeV$)$	0.00	2.1×10^{-4}	1.7×10^{-3}
$\chi\chi \longrightarrow c\bar{c}$			
$N_\gamma(>10$ GeV$)$	7.10	10.61	12.71
$N_\gamma(>50$ GeV$)$	0.69	1.60	2.19
$N_\gamma(>100$ GeV$)$	0.11	0.41	0.66
$N_\gamma(>500$ GeV$)$	0.00	8.7×10^{-5}	8.4×10^{-4}
$\chi\chi \longrightarrow t\bar{t}$			
$N_\gamma(>10$ GeV$)$	5.03	8.65	10.81
$N_\gamma(>50$ GeV$)$	0.29	0.84	1.29
$N_\gamma(>100$ GeV$)$	0.04	0.17	0.30
$N_\gamma(>500$ GeV$)$	0.00	1.7×10^{-4}	8.1×10^{-4}
$\chi\chi \longrightarrow b\bar{b}$			
$N_\gamma(>10$ GeV$)$	7.02	11.02	13.31
$N_\gamma(>50$ GeV$)$	0.49	1.26	1.83
$N_\gamma(>100$ GeV$)$	0.07	0.28	0.47
$N_\gamma(>500$ GeV$)$	0.00	5.8×10^{-5}	6.3×10^{-4}
$\chi\chi \longrightarrow$ gluons			
$N_\gamma(>10$ GeV$)$	6.42	10.69	13.18
$N_\gamma(>50$ GeV$)$	0.34	0.95	1.47
$N_\gamma(>100$ GeV$)$	0.04	0.17	0.32
$N_\gamma(>500$ GeV$)$	0.00	5.7×10^{-5}	4.3×10^{-4}

photons produced in each pure final state for different threshold energies. This information may be used to make predictions for the gamma-ray fluxes also for DM candidates other than the neutralino.

The results of this section and of Sec. III will be used in the next sections to predict the photon fluxes from the galactic center and from our representative external galaxies.

V. PREDICTION AND DETECTABILITY OF PHOTON FLUXES

In this section we will show the results on the prediction of photon fluxes from neutralino annihilation in our Galaxy and in some selected external galaxies. We will therefore study the detectability of such signals with ground-based Čerenkov telescopes and next generation satellite-borne experiments.

TABLE VIII. Integrated number of photons above a given energy E from the annihilation of neutralinos with masses 500 GeV, 800 GeV, and 1 TeV, for different channels of annihilation.

	$m_\chi = 500$ GeV	$m_\chi = 800$ GeV	$m_\chi = 1$ TeV
$N_\gamma(>500$ GeV$)$	0.00	5.8×10^{-5}	6.3×10^{-4}
	$\chi\chi \longrightarrow \tau^+\tau^-$		
$N_\gamma(>10$ GeV$)$	2.19	2.38	2.46
$N_\gamma(>50$ GeV$)$	1.16	1.55	1.72
$N_\gamma(>100$ GeV$)$	0.58	0.98	1.28
$N_\gamma(>500$ GeV$)$	0.00	3.3×10^{-2}	8.2×10^{-2}
	$\chi\chi \longrightarrow W^+W^-$		
$N_\gamma(>10$ GeV$)$	4.76	7.15	8.45
$N_\gamma(>50$ GeV$)$	0.52	1.14	1.57
$N_\gamma(>100$ GeV$)$	0.11	0.34	0.52
$N_\gamma(>500$ GeV$)$	0.00	1.3×10^{-3}	4.4×10^{-3}
	$\chi\chi \longrightarrow ZZ$		
$N_\gamma(>10$ GeV$)$	4.96	7.67	9.19
$N_\gamma(>50$ GeV$)$	0.48	1.12	1.57
$N_\gamma(>100$ GeV$)$	0.09	0.30	0.49
$N_\gamma(>500$ GeV$)$	0.00	0.9×10^{-3}	3.1×10^{-3}

## A. Predicted photon fluxes from neutralino annihilation

In the previous sections we have computed the cosmological factor Φ^{cosmo} (see Fig. 2) and the supersymmetric factor Φ^{SUSY} (see Fig. 8). We are now ready to predict the gamma-ray fluxes from neutralino annihilation in the

TABLE IX. Integrated number of photons above a given energy E from the annihilation of 1 TeV neutralino into a sample state of Higgs bosons, with subsequent decay into b quarks or tau leptons. A mass of 120 GeV has been assumed for the light Higgs, while a mass of 500 GeV has been taken for the charged, heavy and pseudoscalar Higgs's.

$\chi\chi \longrightarrow$ Higgs	
$hh \to b\bar{b}$	$hh \to \tau^+\tau^-$
$N_\gamma(>10$ GeV$)$ 13.95	3.89
$N_\gamma(>50$ GeV$)$ 1.56	1.97
$N_\gamma(>100$ GeV$)$ 0.34	1.07
$N_\gamma(>500$ GeV$)$ 1.8×10^{-4}	0.02
$AA(HH) \to b\bar{b}$	$AA(HH) \to \tau^+\tau^-$
$N_\gamma(>10$ GeV$)$ 13.32	4.00
$N_\gamma(>50$ GeV$)$ 1.37	2.01
$N_\gamma(>100$ GeV$)$ 0.27	1.09
$N_\gamma(>500$ GeV$)$ 6.8×10^{-5}	0.02
$H^+H^- \to b\bar{b}$	$H^+H^- \to \tau^+\tau^-$
$N_\gamma(>10$ GeV$)$ 11.41	2.00
$N_\gamma(>50$ GeV$)$ 1.00	1.00
$N_\gamma(>100$ GeV$)$ 0.17	0.54
$N_\gamma(>500$ GeV$)$ 7.4×10^{-5}	0.01

effective MSSM. Results are reported in Figs. 9 and 10, where we show the expected fluxes of γ rays with energies above 50 GeV and 100 GeV from the galactic center and M31 and for a detector aperture of $\Delta\Omega = 10^{-5}$ sr. Figure 9 refers to the galactic center for a Milky Way with an NFW97 density profile, while Fig. 10 is calculated for M31 with an M99 density profile. The spread of points is given by the different SUSY parameters corresponding to each point.

In the case of the flux from the galactic center with an NFW97 profile and a typical threshold energy of 50 GeV, we predict a maximal gamma-ray flux of the order of 10^{-12} cm^{-2} s^{-1} for neutralinos lighter than 200 GeV, while heavier neutralinos can provide a maximal flux of
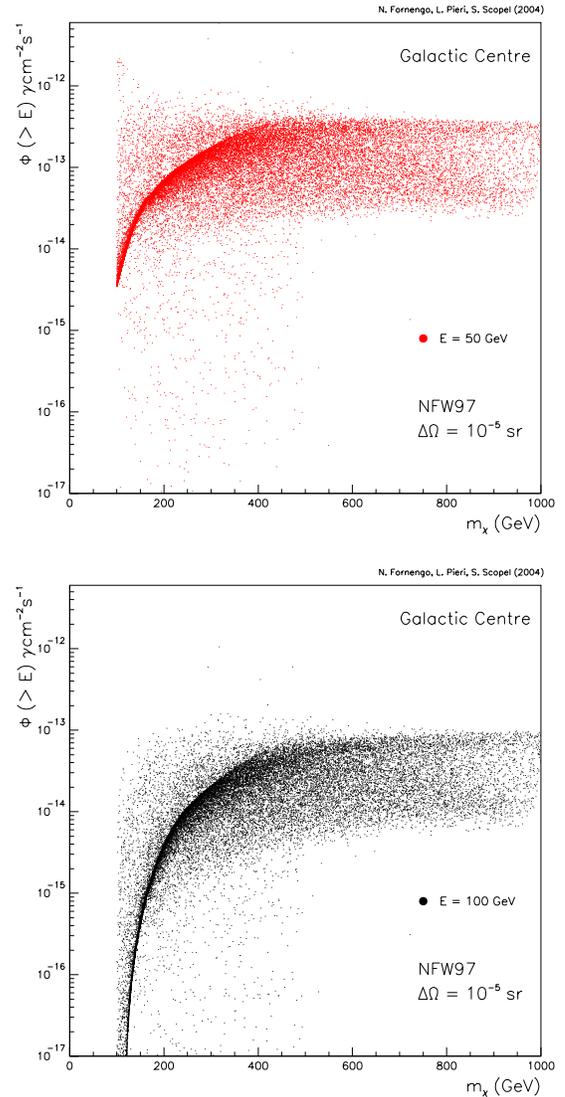
FIG. 9 (color online). Integrated gamma-ray fluxes from neutralino annihilation at the galactic center, for an NFW97 density profile and inside a solid angle $\Delta\Omega = 10^{-5}$ sr. Two representative threshold energies have been assumed: 50 GeV (upper panel) and 100 GeV (lower panel).
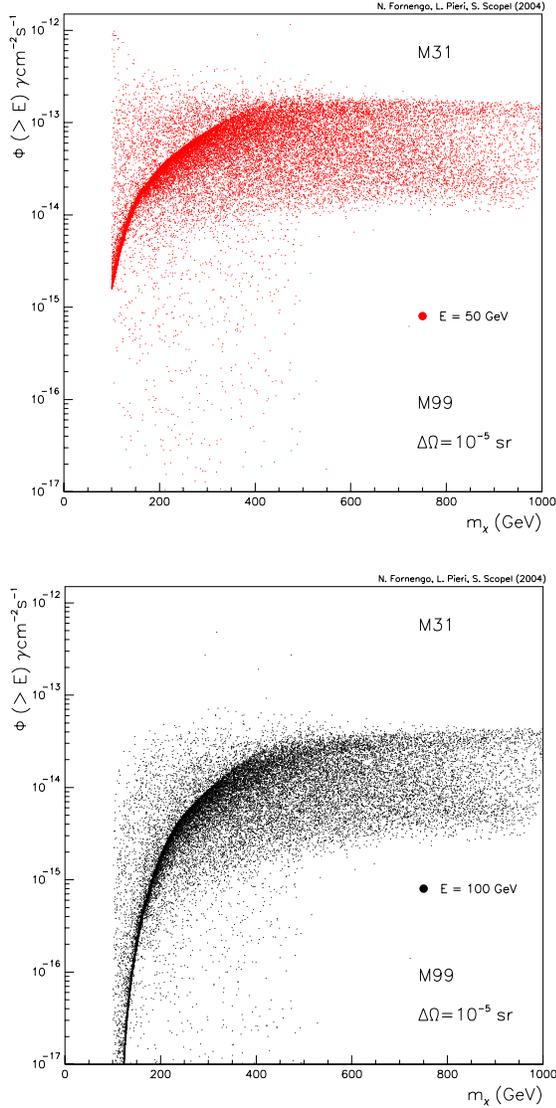
FIG. 10 (color online). Integrated gamma-ray fluxes from neutralino annihilation in M31, for an M99 density profile and inside a solid angle $\Delta\Omega = 10^{-5}$ sr. Two representative threshold energies have been assumed: 50 GeV (upper panel) and 100 GeV (lower panel).

the order of a few 10^{-13} cm^{-2} s^{-1}. In the case of an M99 density profile toward the galactic center, the fluxes are increased by a factor of about 160, as can be deduced from Fig. 3. In this case the maximal fluxes can reach the level of 10^{-10} cm^{-2} s^{-1}. If the detector threshold energy is increased to 100 GeV the gamma-ray fluxes are 1 order of magnitude smaller. Finally, as a consequence of the previously discussed property of Φ^{SUSY}, we see that for neutralino masses heavier than about 500 GeV the supersymmetric models we are considering provide gamma-ray fluxes inside a band with a lower limit of a few 10^{-14} cm^{-2} s^{-1}, for an NFW97 profile. Obviously, if we enlarge the allowed intervals for the MSSM parameters (our definitions are given in Sec. IV), lower gamma-ray

fluxes can be obtained also for heavy neutralinos. However, if we consider natural mass scales for the supersymmetric model, which means that we should not increase the scale of the mass parameters of the model much over the TeV scale, Fig. 9 shows the level of the lower limit on the gamma-ray flux for heavy neutralinos.

Also the Andromeda Galaxy can provide gamma-ray fluxes of the order of 10^{-12}–10^{-13} cm^{-2} s^{-1} inside a solid angle of $\Delta\Omega = 10^{-5}$ sr, but only for an M99 density profile. These values therefore represent the maximal fluxes which can be produced by neutralino annihilation in M31. We remind that although the galactic center is much brighter for the same density profile, M31 can be resolved over the galactic gamma-ray signal due to its location at $\psi = 119°$, as is shown in Fig. 2.

In the following we will compare our expected fluxes with the sensitivity curves of foreseeable experiments.

B. Detectability of photon fluxes from neutralino annihilation

We have considered two platforms of observations of γ rays from neutralino annihilation, corresponding to a Čerenkov apparatus with the characteristics of VERITAS [1] and to a satellite-borne experiment similar to GLAST [4]. The detectability of the diffuse flux from DM annihilation is computed by comparing the number n_γ of expected γ events with the fluctuations of background events n_{bkg}. To this purpose we define the following ratio σ given by:

$$\sigma \equiv \frac{n_\gamma}{\sqrt{n_{\text{bkg}}}}$$
$$= \frac{\sqrt{T_\delta}\epsilon_{\Delta\Omega}}{\sqrt{\Delta\Omega}} \frac{\int A_\gamma^{\text{eff}}(E,\theta)[d\phi_\gamma^{\text{DM}}/dEd\Omega]dEd\Omega}{\sqrt{\int \sum_{\text{bkg}} A_{\text{bkg}}^{\text{eff}}(E,\theta)[d\phi_{\text{bkg}}/dEd\Omega]dEd\Omega}}$$

(12)

where T_δ defines the effective observation time and ϕ_{bkg} is the background flux. For a Čerenkov apparatus, for instance, it is defined as the time during which the source is seen with zenith angle $\theta \leq 60°$. The quantity $\epsilon_{\Delta\Omega} = 0.7$ is the fraction of signal events within the optimal solid angle $\Delta\Omega$ corresponding to the angular resolution of the instrument. The effective detection areas A^{eff} for electromagnetic and hadronic induced showers are defined as the detection efficiency times the geometrical detection area. For the case of a Čerenkov apparatus we have assumed a conservative effective area $A^{\text{eff}} = 4 \times 10^8$ cm^2, while for a satellite experiment we have considered $A^{\text{eff}} = 10^4$ cm^2. Both values have been assumed independent from E and θ. Note that while the former can be increased by adding together more Čerenkov telescopes, the latter is intrinsically limited by the size of the satellite and cannot be much greater than the fiducial value quoted here. Finally we have assumed an angular resolution of 0.1°

for both instruments, and a total effective pointing time of 20 days for the Čerenkov telescope and 30 days for the experiment on satellite. An identification efficiency ϵ must be taken into account, which is one of the most important factors which have to be studied in order to reduce the physical background level. A Čerenkov apparatus has a typical identification efficiency for electromagnetic induced (primary γ or electron) showers $\epsilon_{\text{e.m.}} \sim 99\%$ and for hadronic showers $\epsilon_{\text{had}} \sim 99\%$. This means that only one hadronic shower out of 100 is misidentified as an electromagnetic shower. Unfortunately, this method cannot distinguish between primary photons and electrons, which therefore represent an irreducible background for ground-based detectors. As far as a satellite-borne experiment is concerned, an identification efficiency for charged particles of $\epsilon_{\text{charged}} \sim 99.997\%$ can be assumed, while for photons it lowers to $\epsilon_{\text{neutral}} \sim 90\%$ due to the backsplash of high energy photons [62].

We have considered the following values for the background levels. For the proton background we use [63]:

$$\frac{d\phi^h}{d\Omega dE} = 1.49 E^{-2.74} \frac{p}{\text{cm}^2\,\text{s sr GeV}}, \qquad (13)$$

while for the electron background [64]:

$$\frac{d\phi^e}{d\Omega dE} = 6.9 \times 10^{-2} E^{-3.3} \frac{e}{\text{cm}^2\,\text{s sr GeV}} \qquad (14)$$

and finally for the Galactic photon emission, as extrapolated by EGRET data at lower energies, we employ [13]:

$$\frac{d\phi^{\text{gal}-\gamma}_{\text{diffuse}}}{d\Omega dE} = N_0(l,b) 10^{-6} E_\gamma^\alpha \frac{\gamma}{\text{cm}^2\,\text{s sr GeV}}, \qquad (15)$$

with α set to -2.7 in the considered energy range, with lack of data for energies higher than tens of GeV. The normalization factor N_0 depends only on the interstellar matter distribution, and is modeled as [13]:

$$N_0(l,b) = \frac{85.5}{\sqrt{1+(l/35)^2}\sqrt{1+[b/(1.1+|l|0.022)]^2}} + 0.5 \qquad (16)$$

for $|l| \geq 30°$ and

$$N_0(l,b) = \frac{85.5}{\sqrt{1+(l/35)^2}\sqrt{1+(b/1.8)^2}} + 0.5 \qquad (17)$$

for $|l| \leq 30°$, where the longitude l and the latitude b are assumed to vary in the intervals $-180° \leq l \leq 180°$ and $-90° \leq b \leq 90°$, respectively. Finally, for the diffuse extragalactic γ emission, as extrapolated from EGRET data at lower energies [65], we use:

$$\frac{d\phi^{\text{extra}-\gamma}_{\text{diffuse}}}{d\Omega dE} = 1.38 \times 10^{-6} E^{-2.1} \frac{\gamma}{\text{cm}^2\,\text{s sr GeV}}. \qquad (18)$$

If a galactic origin of high galactic latitude γ emission is considered, then this last estimate should be increased by about 60% [66].

Figure 11 shows the five σ sensitivity curves for the experimental apparata discussed above. Because of the different γ backgrounds, the curves are slightly different in the direction of the galactic center or toward the M31
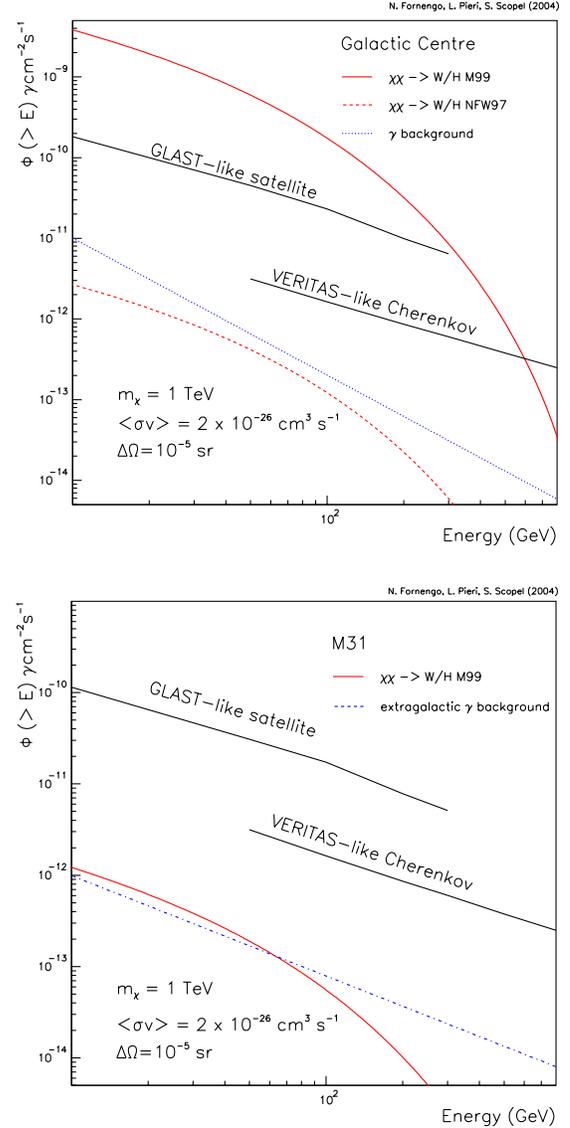

FIG. 11 (color online). Study of the sensitivity of an ACT detector and a satellite-borne experiment to photon fluxes from a TeV neutralino annihilation. Solid lines denote the 5σ sensitivity curves for satellite and Čerenkov detectors. These curves have been calculated according to the prescriptions given in the text. The flux expected from the galactic center with an NFW97 and an M99 profile are shown in the upper panel. The flux from M31 with an M99 profile is shown in the lower panel. Photon fluxes are given for $\Delta\Omega = 10^{-5}$ sr, which is the typical detector acceptance.

galaxy. Also plotted for reference is the expected integrated γ-ray flux for a SUSY model with $m_\chi = 1$ TeV, 50% branching ratio of annihilation into W bosons and 50% into Higgs bosons (following the results of Fig. 6 for the branching ratios of high mass neutralinos), and an annihilation cross section of 2×10^{-26} cm^3 s^{-1} which refers to the most optimistic values of Figs. 9 and 10. Because of our discussion in the previous section on the properties of Φ^{SUSY}, one could then consider the curve of γ-ray flux from neutralino annihilation which we show in Fig. 11 as the highest spectrum of a range of curves given by the spread of points in Figs. 9 and 10.

From Fig. 11 and our previous discussion on the cosmological and supersymmetric factor it therefore arises that signals from extragalactic objects could hardly be detected. The gamma-ray spectrum calculated for an M99 profile is 2 orders of magnitude smaller than the expected sensitivities we estimate for detectors like GLAST and about 1 order of magnitude smaller than the estimated sensitivity of VERITAS. We also notice that the most optimistic prediction for the flux we are showing in Fig. 11 is at the level of the extrapolated background, a fact which by itself would make problematic the observation of a signal from M31. Only in the very optimistic case of a clumpy M99 matter density, would the expected signal exceed the extrapolated background, but it would nevertheless remain inaccessible.

In the case of a signal from the galactic center, a density profile as cuspy as M99 (or the adiab-NFW) could be resolved by both a satellite detector like GLAST and a Čerenkov telescope with the characteristics of VERITAS. In the case of an NFW97 profile, a potential signal would not be accessible. Therefore, in the case of the signal from the galactic center a density profile harder than NFW97 is required in order to have a signal accessible to GLAST-like and VERITAS-like detectors.

C. Comparison with recent data

Recent experimental data taken from CANGAROO-II [6] in the direction of the galactic center show that the spectral shape of photons from the galactic center is in excess of the extrapolated background from standard processes. Figure 12 shows the CANGAROO-II data in the right panel, and the EGRET data [5] at lower energies in the left panel. We have superimposed on the data the γ-ray background used in our previous analysis, as well as the predicted γ-ray spectra from high mass neutralino annihilation, for the NFW97 and the M99 profiles. These spectra have been normalized within a solid angle coherent with the observations. We can see that not even an M99 profile can reproduce the observed data, as already observed in Ref. [67]. Figure 13 reproduces the same information of Fig. 12, but the cosmological factor has been enhanced by a factor 2.5 (equivalently, one could think to an enhancement in the supersymmetric factor,

but this is not possible in the effective MSSM, neither in more constrained minimal SUGRA models which usually provide annihilation cross sections smaller than the effective MSSM). However, in the case of a DM pull-in induced by the presence of baryons, an M99 profile could easily account for the CANGAROO-II data. We can also see that, when appropriately boosted, the signals from annihilation of neutralinos with mass higher than 1 TeV have the property of matching the observed CANGAROO-II data and not being in conflict with the EGRET data.

On the other hand, Fig. 12 shows that it is not possible to explain at the same time both the EGRET excess in the 1–20 GeV energy range and the CANGAROO-II flux at energies above 250 GeV with the spectral shape of a gamma-ray flux from neutralino annihilation. While the EGRET spectrum can be well explained by a light neutralino in a nonuniversal gaugino model [7], with $m_\chi \sim$ 30–40 GeV, or by a neutralino of about 50–60 GeV [68]
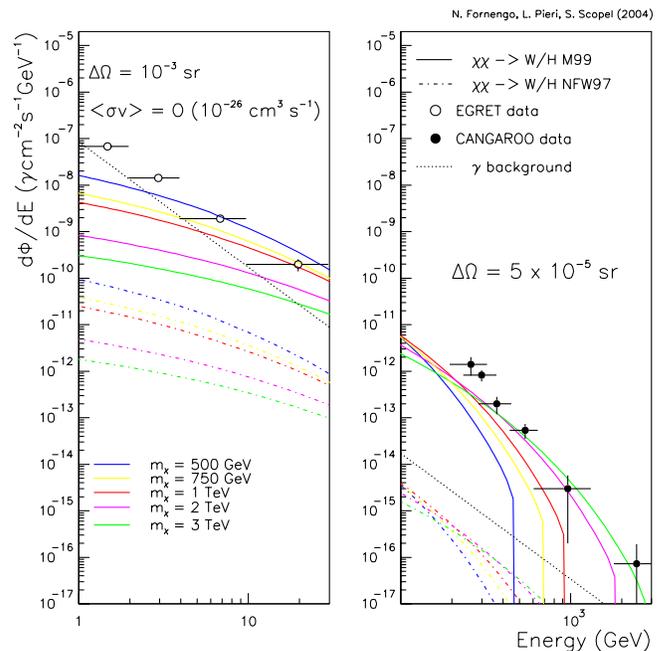

FIG. 12 (color online). Differential spectrum of the photon flux expected from neutralino annihilation in the galactic center. A 50% branching ratio into W pairs and 50% into b quarks has been assumed. Solid lines represent the calculation for an M99 profile for different neutralino masses, while dash-dotted lines show the same spectra assuming an NFW97 profile. Dotted lines show the extrapolated γ-ray "conventional" background. Open circles (left panel) show the EGRET results on photon flux from the galactic center, while filled circles (right panel) show the recent data at higher energies from CANGAROO-II. Photon fluxes are given for the corresponding typical detector acceptance, that is for $\Delta\Omega = 10^{-3}$ sr in the left panel and for $\Delta\Omega = 5 \times 10^{-5}$ sr in the right panel.
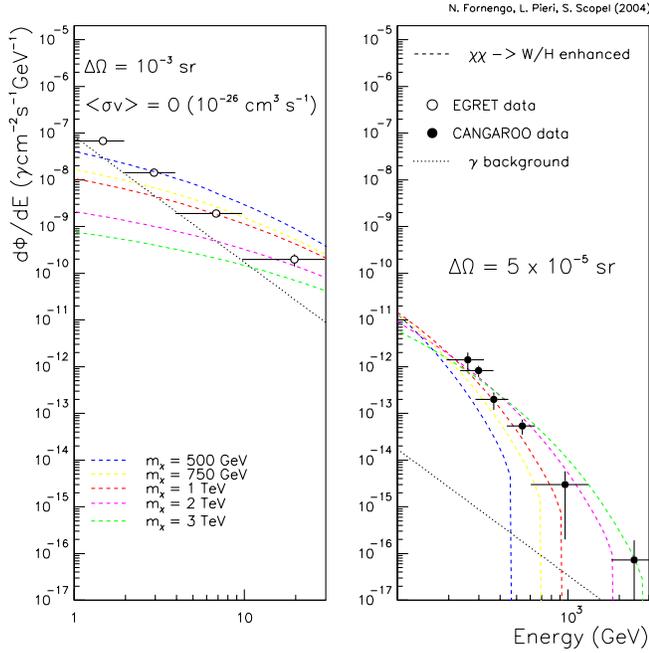
FIG. 13 (color online). The same as in Fig. 12 for an M99 profile multiplied by a factor 2.5 (dashed lines).

in the effective MSSM, the CANGAROO-II data require much heavier neutralinos in order to produce photons in the hundreds of GeV range: in this case, however, the
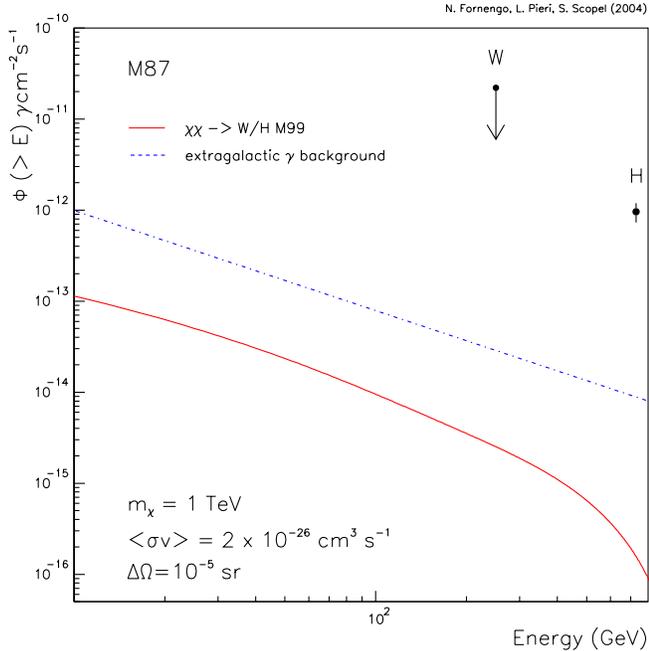

FIG. 14 (color online). Integrated photon flux as expected from a TeV neutralino annihilation in the M87 galaxy. Photon fluxes are given for $\Delta\Omega = 10^{-5}$ sr, which is the typical detector acceptance. Also shown in the figure is the upper limit determined by WHIPPLE [70] and the measurement from HEGRA [69].

ensuing gamma-ray spectra are too low in the 1–10 GeV range and cannot reproduce the EGRET data together with the CANGAROO-II ones.

We complete this section by applying our method to M87 and comparing our results with the measurements available for that galaxy, which show a possible indication of a γ-ray excess. This is shown in Fig. 14, where one can see that our predictions are well below the flux measured by HEGRA [69], even if an M99 profile is assumed. Not even a clumpy distribution, which could enhance the predicted fluxes by at most a factor of 5, would allow us to explain the HEGRA excess by means of neutralino annihilations in the effective MSSM.

VI. CONCLUSIONS

We have discussed the gamma-ray signal from dark matter annihilation in our Galaxy and in external objects, namely, the Large Magellanic Cloud, the Andromeda Galaxy (M31), and M87. The aim of our paper was to derive consistent predictions for the fluxes in a specific realization of supersymmetry, the effective MSSM, and to compare the predictions with the capabilities of new-generation satellite-borne experiments, like GLAST, and ground-based Čerenkov telescopes, for which we have used, for definiteness, the characteristics of the VERITAS telescope.

Our results show that only the signal from neutralino annihilation at the galactic center could be accessible to
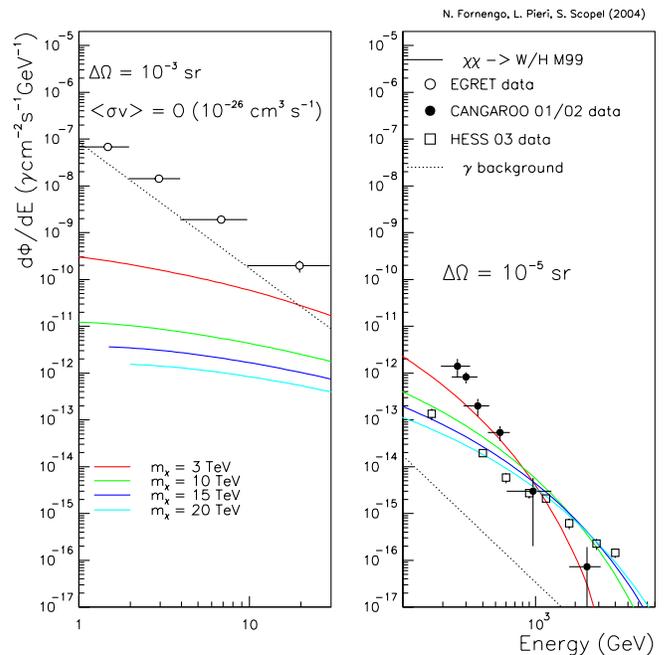

FIG. 15 (color online). The same as in Fig. 12, including the data from HESS [71] (see *Note Added* at the end of the paper). Photon fluxes are shown for neutralino masses up to 20 TeV and for an M99 density profile.

both satellite-borne experiments and to ACTs, even though this requires very steep dark matter density profiles toward the galactic center. A profile steeper than NFW97 is required in order to provide signals which can reach detectable levels. In the case of signals coming from external galaxies, even though the extragalactic signal is larger than the galactic contribution from neutralino annihilation, the absolute level of the flux is too low to allow detection with the experimental techniques currently under development.

We have also compared our theoretical predictions with the recent CANGAROO-II data from the galactic center and with the HEGRA data from M87. In both cases an indication of a gamma-ray excess is present. In the case of the CANGAROO-II data, the spectral shape is well reproduced by a gamma-ray flux from annihilation of neutralinos somewhat heavier than about 1 TeV, in agreement with Ref. [67]. However the overall normalization of the flux requires a boost factor of about 2.5 over the flux obtained with a Moore *et al.* profile: this seems hard to obtain even in the presence of clumps. On the other hand, we notice that in the case of a DM pull-in induced by the presence of baryons, as discussed in Sec. III A 2, the data could be easily explained by a Moore *et al.* profile, without the necessity to invoke strong clumpiness. We also showed that the agreement with the CANGAROO-II data which is obtained with these boosted fluxes is not in contrast with the lower-energy EGRET data from the galactic center. In addition we showed that the spectral features of such fluxes cannot explain at the same time both the CANGAROO-II and EGRET excess by invoking a very heavy neutralino. Finally, we compared our predictions for the signal from M87 with the HEGRA data and found that the predicted fluxes from neutralino annihilation are too low to explain the HEGRA result.

Note added.—The HESS Čerenkov telescope [71] has recently published new data on gamma rays from the galactic center. The measured flux and spectrum differ substantially from previous results, in particular those reported by the CANGAROO Collaboration, exhibiting a much harder power-law energy spectrum, with spectral index of about -2.2. According to our analysis, these data, if interpreted in terms of neutralino annihilation, would require a neutralino mass in the range $10 \text{ TeV} \lesssim m_\chi \lesssim 20 \text{ TeV}$ and an M99 profile for the DM distribution, as shown in Fig. 15.

[1] T. C. Weekes *et al.*, in *Proceedings of the 25th ICRC*, edited by M. S. Potgieter, B. C. Raubenheimer, and D. J. van der Walt (World Scientific, Singapore, 1998).

[2] F. A. Aharonian *et al.*, Astropart. Phys. **6**, 343 (1997).

[3] C. Baixeras *et al.*, Nucl. Phys. B, Proc. Suppl. **114**, 247, (2003).

[4] A. Morselli *et al.*, in *Proceedings of the 32nd Rencontres de Moriond*, edited by Y. Giraud-Heraud and J. Tran Thanh Van (Edition Frontieres, Paris, France, 1997).

[5] S. D. Hunter *et al.*, Astrophys. J. **481**, 205 (1997).

[6] CANGAROO-II Collaboration, K. Tsuchiya *et al.*, Astrophys. J. **606**, L115 (2004).

[7] A. Bottino, F. Donato, N. Fornengo, and S. Scopel, Phys. Rev. D **70**, 015005 (2004).

[8] H. Bengtsson, P. Salati, and J. Silk, Nucl. Phys. **B346**, 129 (1990); V. Berezinsky, A. Bottino, and G. Mignola, Phys. Lett. B **325**, 136 (1994); P. Chardonnet *et al.*, Astrophys. J. **454**, 774 (1995); G. Jungman and M. Kamionkowsky, Phys. Rev. D **51**, 3121 (1995); L. Bergström, J. Edsjö, and P. Ullio, Phys. Rev. D **58**, 083507 (1998); L. Bergström, J. Edsjö, P. Gondolo, and P. Ullio, Phys. Rev. D **59**, 043506 (1998); L. Bergström, P. Ullio, and J. Buckley, Astropart. Phys. **9**, 137 (1998); P. Ullio and L. Bergström, Nucl. Phys. **B504**, 27 (1997); Phys. Rev. D **57**, 1962 (1998); P. Gondolo and J. Silk, Phys. Rev. Lett. **83**, 1719 (1999); C. Calcaneo–Roldan and B. Moore, Phys. Rev. D **62**, 123005 (2000); G. Bertone, G. Sigl, and J. Silk, Mon. Not. R. Astron. Soc. **326**, 799 (2001); P. Ullio, J. High Energy Phys. 06 (2001) 053; P. Ullio, H. S. Zhao, and M. Kamionkowski, Phys. Rev. D **64**, 043504 (2001); P. Ullio, L. Bergström, J. Edsjo, and C. G. Lacey, Phys. Rev. D **66**, 123502 (2002); D. Hooper and B.L. Dingus, astro-ph/0210617; J. Buckley *et al.*, astro-ph/0201160; L. Bergström, J. Edsjo, and P. Ullio, Phys. Rev. Lett. **87**, 251301 (2001); L. Bergström, J. Edsjo, and C. Gunnarsson, Phys. Rev. D **63**, 083515 (2001); J. L. Feng, K. T. Matchev, and F. Wilczek, Phys. Rev. D **63**, 045024 (2001); A. Cesarini, F. Fucito, A. Lionetto, A. Morselli, and P. Ullio, Astropart. Phys. **21**, 267 (2004); R. Aloisio, P. Blasi, and A.V. Olinto, J. Cosmol. Astropart. Phys. 05 (2004) 007; R. Aloisio, P. Blasi, and A.V. Olinto, Astrophys. J. **601**, 47 (2004); D. Elsaesser and K. Mannheim, Astropart. Phys. **22**, 65 (2004); astro-

ph/0405235; S. Peirani, P. Mohayaee, and J. A. de Freitas Pacheco, Phys. Rev. D **70**, 043503 (2004).

[9] F. Stoehr, S. D. M. White, V. Springel, G. Tormen, and N. Yoshida, Mon. Not. R. Astron. Soc. **345**, 1313 (2003).

[10] Y. Mambrini and C. Muñoz, hep-ph/0407158.

[11] L. Pieri and E. Branchini, Phys. Rev. D **69**, 043512 (2004).

[12] E. A. Baltz, C. Briot, P. Salati, R. Taillet, and J. Silk, Phys. Rev. D **61**, 023514 (2000).

[13] L. Bergström et al., Astropart. Phys. **9**, 137 (1998).

[14] J. F. Navarro et al., Astrophys. J. **490**, 493 (1997).

[15] B. Moore et al., Astrophys. J. Lett. **524**, L19 (1999).

[16] V. R. Eke et al., Astrophys. J. **554**, 114 (2001).

[17] J. Diemand, B. Moore and J. Stadel, astro-ph/0402267.

[18] P. Ullio, H. Zhao, and M. Kamionkowski, Phys. Rev. D **64**, 043504 (2001).

[19] J. F. Navarro et al., Mon. Not. R. Astron. Soc. **349**, 1039 (2004).

[20] F. Stoehr, astro-ph/0403077.

[21] F. Stoehr, S. D. M. White, V. Springel, G. Tormen, and N. Springel, Mon. Not. R. Astron. Soc. **335**, L84 (2002).

[22] D. A. Buote, International Astronomical Union Symp. 220 No. 149 (2004).

[23] M. W. Bautz and J. S. Arabadjis, astro-ph/0303313.

[24] W. J. G. de Blok, A. Bosma, and S. McGaugh, Mon. Not. R. Astron. Soc. **340**, 657 (2003).

[25] D. J. Sand et al., astro-ph/0309465.

[26] E. Hayashi et al., astro-ph/0310576.

[27] C. Power et al., Mon. Not. R. Astron. Soc. **338**, 14 (2003).

[28] R. A. Swaters et al., Astrophys. J. **583**, 732 (2003).

[29] See for instance: F. Donato, G. Gentile, and P. Salucci, astro-ph/0403206; A. Borriello and P. Salucci, Mon. Not. R. Astron. Soc. **323**, 295 (2001).

[30] H. Dahle, astro-ph/0310549.

[31] M. R. Merrifield, astro-ph/0310497.

[32] P. Gondolo and J. Silk, Phys. Rev. Lett. **83**, 1719 (1999).

[33] O. Y. Gnedin, A. V. Kravtsov, A. A. Klypin, and D. Nagai, astro-ph/0401512.

[34] F. Prada, A. Klyplin, J. Flix, M. Martínez, and E. Simonneau, astro-ph/0406247.

[35] D. Merritt, M. Milosavljević, L. Verde, and R. Jimenez, Phys. Rev. Lett. **88**, 191301 (2002).

[36] D. Merritt, Phys. Rev. Lett. **92**, 201304 (2004).

[37] A. S. Ilyin, K. P. Zybin, and A. V. Gurevic, Zh. Eksp. Teor. Fiz. **98**, 5 (2004) [J. Exp. Theor. Phys. **98**, 1 (2004)].

[38] V. Berezinsky et al., Phys. Lett. B **294**, 221 (1992).

[39] V. Berezinsky et al., Phys. Rev. D **68**, 103003 (2003).

[40] A. Helmi, S. White, and V. Springel, Mon. Not. R. Astron. Soc. **339**, 834 (2003).

[41] S. Ghigna et al., Astrophys. J. **544**, 616 (2000).

[42] P. Blasi and R. K. Sheth, Phys. Lett. B **486**, 233 (2000).

[43] R. Aloisio, P. Blasi, and A. V. Olinto, Astrophys. J. **601**, 47 (2004).

[44] C. Calcaneo-Roldan and B. Moore, Phys. Rev. D **62**, 123005 (2000).

[45] L. Pieri and E. Branchini (to be published).

[46] LEPSUSY Working Group, ALEPH, DELPHI, L3 and OPAL experiments, http://lepsusy.web.cern.ch/lepsusy/Welcome.html.

[47] A. Bottino, N. Fornengo, and S. Scopel, Phys. Rev. D **67**, 063519 (2003); A. Bottino, F. Donato, N.Fornengo, and S. Scopel, Phys. Rev. D **68**, 043506 (2003); Phys. Rev. D **69**, 037302 (2003).

[48] LEP Higgs Working Group, http://lephiggs.web.cern.ch/LEPHIGGS /www/Welcome.html.

[49] CLEO Collaboration, S. Ahmed et al., hep-ex/9908022; ALEPH Collaboration, R. Barate et al., Phys. Lett. B **429**, 169 (1998); Belle Collaboration, K. Abe et al., Phys. Lett. B **511**, 151 (2001).

[50] CDF Collaboration, D. Acosta et al., Phys. Rev. Lett. **93**, 032001 (2004).

[51] M. Davier et al., Eur. Phys. J. C **31**, 503 (2003).

[52] K. Hagiwara, A. D. Martin, D. Nomura, and T. Teubner, Phys. Rev. D **69**, 093003 (2004).

[53] M. Ciuchini, G. Degrassi, P. Gambino, and G. F. Giudice, Nucl. Phys. **B527**, 21 (1998); **B534**, 3 (1998); M. Carena, D. Garcia, U. Nierste, and C. E. M. Wagner, Phys. Lett. B **499**, 141 (2001).

[54] C. Bobeth, T. Ewerth, F. Krüger, and J. Urban, Phys. Rev. D **64**, 074014 (2001); A. Dedes, H. K. Dreiner, and U. Nierste,Phys. Rev. Lett. **87**, 251804 (2001).

[55] M. Carena, D. Garcia, U. Nierste, and C. E. M. Wagner, Phys. Lett. B **499**, 141 (2001) and references quoted therein.

[56] D. N. Spergel et al., Astrophys. J. Suppl. Ser. **148**, 175 (2003).

[57] SDSS Collaboration, M. Tegmark et al., Phys. Rev. D **69**, 103501 (2004).

[58] A. Bottino, V. de Alfaro, N. Fornengo, G. Mignola, and M. Pignone, Astropart. Phys. **2**, 67 (1994).

[59] K. Griest and D. Seckel, Phys. Rev. D **43**, 3191 (1991); S. Mizuta and M. Yamaguchi, Phys. Lett. B **298**, 120 (1993); J. Edsjo and P. Gondolo, Phys. Rev. D **56**, 1879 (1997); J. R. Ellis, T. Falk, and K. A. Olive, Phys. Lett. B **444**, 367 (1998).

[60] F. Donato, N. Fornengo, D. Maurin, P. Salati, and R. Taillet, Phys. Rev. D **69**, 063501 (2003).

[61] T. Sjöstrand, P. Eden, C. Friberg, L. Lonnblad, G. Miu, S. Mrenna, and E. Norrbin, Comput. Phys. Commun. **135**, 238 (2001).

[62] A. Moiseev et al., in Proceedings of ICRC 2003, edited by T. Kajita, Y. Asaoka, A. Kawachi, Y. Matsubara, and M. Sasaki (Univ. Acad. Pr., Tokyo, 2003).

[63] Copernicus Group, T. Gaisser et al., in Proceedings of the 27th ICRC, edited by R. Schlickheiser (Katlenburg-Lindau, Germany, 2001).

[64] M. S. Longair, High Energy Astrophysics (Cambridge University Press, Cambridge, England, 1992).

[65] P. Sreekumar et al., Astrophys. J. **494**, 523, (1998).

[66] A. Dar and A. De Rújula, Mon. Not. R. Astron. Soc. **323**, 391 (2001).

[67] D. Hooper et al., J. Cosmol. Astropart. Phys. 09 (2004) 002.

[68] Alessandro Cesarini, Francesco Fucito, Andrea

Lionetto, Aldo Morselli, and Piero Ullio, Astropart. Phys. **21**, 267 (2004).

[69] N. Götting *et al.*, in *Proceedings of the 28th ICRC*, edited by T. Kajita, Y. Asaoka, A. Kawachi, Y. Matsubara, and M. Sasaki (Univ. Acad. Pr., Tokyo, 2003).

[70] Copernicus Group, S. Lebohec *et al.*, in *Proceedings of the 27th ICRC*, edited by R. Schlickheiser (Katlenburg-Lindau, Germany, 2001).

[71] The HESS Collaboration, F. Aharonian *et al.*, astro-ph/ 0408145.